

Article pubs.acs.org/JPCC

Time- and Pressure-Dependent Gas Diffusion in a Nanoconfined **Liquid Phase**

Lijiang Xu, † Mingzhe Li, † and Weiyi Lu*



Cite This: J. Phys. Chem. C 2021, 125, 5596-5601



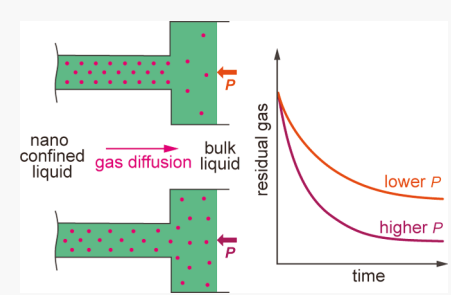
ACCESS I

III Metrics & More

Article Recommendations

Supporting Information

ABSTRACT: Fundamentally understanding the gas-liquid interaction in a nanoenvironment is important in nanofluidics-based systems. Here, a systematically experimental study of the gas diffusion in a liquid phase confined in hydrophobic nanopores is presented. By holding a liquid nanofoam (LN) system at different pressure levels for various time durations, the gas diffusion behavior is quantified by analyzing the degree of liquid outflow from the hydrophobic nanopores. The results show that the gas diffusion progress exhibits an exponentially decaying rate. In addition, distinct from the bulk case, pressure poses a pronounced effect on the gas diffusion in the nanoconfined liquid. These findings extend the knowledge of gas-liquid interactions in nanofluidicsbased systems.



1. INTRODUCTION

Understanding the gas-liquid interaction in a nanoenvironment is of great importance to a number of natural and technical processes, such as shale gas exploitation, 1,2 gasdiffusion electrodes, 3,4 geological carbon dioxide (CO2) sequestration, 5,6 and gas-liquid membrane contactors. 7,8 The dissolved gas diffusion in a pressurized liquid confined in a nanoenvironment plays a key role in these processes. In nanopores with characteristic pore sizes comparable to those of gas and liquid molecules, the classic diffusion theories break down. For instance, the gas solubility in a nanoconfined liquid is much higher than that in a bulk liquid and has been observed in various gas-liquid combinations, including CO2, H2, or CH₄ dissolved in water, n-hexane, or ethanol confined in nanoporous silica, MCM-41, and SBA-15.9-12 This gas oversolubility significantly affects the gas diffusion behavior in a confined nanoenvironment. Besides, the pressure effect on gas diffusion in the bulk liquid is negligible due to the incompressible mean free path of bulk liquid molecules, 13,14 while pressure change results in condensation of liquid molecules 15,16 and gas clusters 17 under a hydrophobic nanoconfinement. These density changes pose a noteworthy impact on the nanoscale gas diffusion process. Li et al. 18 have found that the characteristics of CO2 diffusivity in water under a nanoconfinement are different from those of its bulk counterpart through molecular dynamics (MD) simulation. However, despite the importance of gas diffusion in a nanoconfined liquid, an elucidation of the time- and pressure-dependent diffusion process is currently lacking and experimental studies, which suffered from the technical challenges at the nanoscale, are still scarce.

A recently developed nanofluidics-enabled energy absorption system, referred to as a liquid nanofoam (LN), $^{19-22}$ is a potential platform to experimentally investigate the gas

diffusion behavior in a nanoconfined liquid. LN is composed of a hydrophobic nanoporous medium and a non-wetting liquid phase. The nanopores are initially filled with gas molecules as their hydrophobic surface inhibits the entering of liquid molecules. When the LN system is pressurized to a critical value, the liquid molecules infiltrate into the nanopores and dissolve all the gas molecules. This liquid infiltration process is a novel energy mitigation mechanism with an unprecedented energy absorption efficiency (~100 J/g), nearly 2 orders of magnitude higher than those of traditional materials. 19,23 As the pressure is removed, the spontaneous liquid outflow from the hydrophobic nanopores is driven by the gas-liquid interaction. 21,24 It has been demonstrated that the degree of liquid outflow reduces with the increase in the amount of gas escaped from the nanoconfined liquid to the bulk liquid phase. ^{25,26} Previous studies on this gas transfer from the nanophase to the bulk phase are focused on advection, while the gas diffusion is ignored due to the relatively short time duration of the liquid outflow process. In the current study, the gas diffusion from the nanophase to the bulk phase is thoroughly studied by holding the infiltrated liquid molecules in the hydrophobic nanopores at different peak pressures with variable time durations. The time- and pressure-dependent nanoconfined gas diffusion is then characterized by the macroscopic liquid outflow behavior of LN.

Received: December 20, 2020 Revised: February 4, 2021 Published: March 5, 2021





2. MATERIALS AND METHODS

2.1. Materials and Sample Preparation. The nanoporous material used in the LN system was a hydrophobic silica gel (Fluka 100 C8, Sigma-Aldrich). The material was in the powder form, with a particle size of $40-63~\mu m$. The average pore size, nanopore volume, and Brunauer–Emmett–Teller (BET) surface area were 8.0 nm, 0.43 cm³/g, and 227.4 m²/g, respectively, measured using a surface area and porosity analyzer (ASAP 2020, Micromeritics). The liquid phase in the LN system was a 3.0 M sodium chloride (NaCl) aqueous solution.

The LN samples were prepared by sealing 0.2 g of the hydrophobic silica gel and 0.9 mL of the 3.0 M NaCl aqueous solution in a stainless-steel cell with two O-ring-equipped pistons, as depicted in Figure 1. The diameter of the piston, *d*,

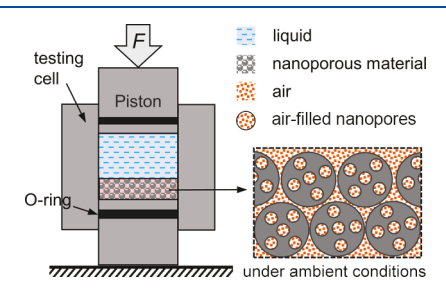


Figure 1. Schematic of an LN sample sealed in a testing cell with two pistons.

was 19 mm. The length of all the LN samples was the same, indicating that the amount of air in the LN samples was a constant.¹⁶ A detailed description of sample preparation is given elsewhere.²⁷

2.2. Pressure-Induced Liquid Infiltration Test. All experiments were conducted at 35 °C in a temperature chamber (Mode 3119-606, Instron). The LN sample sealed in the testing cell was placed on a platen of a universal tester (Mode 5982, Instron). The loading speed of the compression test was 2 mm/min. As the compression progressed, the force F increased and the hydrostatic pressure $P = 4F/\pi d^2$ was built up in the testing cell and exerted on the LN sample. As F reached the preset peak value F_{max} , the Instron load cell was moved back at the same speed. When the load cell returned to its original position, the first loading-unloading cycle was completed. This loading-unloading process was consecutively repeated at least five times for each LN sample. The specific volume change of the LN sample was calculated as $V = \Delta \cdot \pi d^2 / \pi d^2$ 4m, where Δ and m were the measured displacement of the piston and the mass of the nanoporous silica gel, respectively.

2.3. Peak-Pressure-Holding Liquid Infiltration Test. To study the time and pressure dependence of gas diffusion behavior in the nanoconfined liquid, a peak-pressure-holding test was designed. After the completion of the first loading—unloading cycle, the LN sample was compressed to $F_{\rm max}$ at the same loading speed. Then, the LN sample was held at $F_{\rm max}$ for a certain time duration, $t_{\rm h}$, before the load cell was moved back at the same speed in the second cycle. Immediately after the second cycle, a third loading—unloading cycle without holding was applied to characterize the change in the degree of liquid outflow. LN samples with the same composition were held at $F_{\rm max} = 17$ kN, corresponding to a system peak pressure of 60 MPa, for 1.5, 3, 6, 9, 12, and 15 h. For each holding condition, at least three samples were tested. To investigate the pressure

effect on the gas diffusion behavior, another series of peak-pressure-holding tests were performed at $F_{\text{max}} = 43$ kN, equivalent to a system peak pressure of 150 MPa.

3. RESULTS AND DISCUSSION

3.1. Pressure-Induced Liquid Infiltration Tests ($t_h = 0$). Figure 2 shows typical consecutive loading—unloading cycles

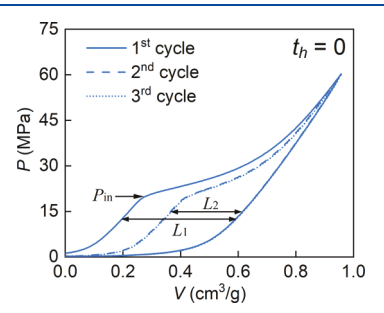


Figure 2. Typical consecutive loading—unloading curves of the LN sample in the pressure-induced liquid infiltration test without the peak-pressure-holding process.

of the LN sample without the peak-pressure-holding process. From the third loading-unloading cycle, the curves are identical to that in the second cycle. For clarity, only the first three consecutive loading-unloading cycles are shown here. Under ambient conditions, the surface energy barrier of the hydrophobic nanopore surface prevents the liquid flowing into the nanopores and the nanopores are initially filled with air, as illustrated in Figure 1. When the system pressure increases, the initial mechanical response of the LN system is elastic with a relatively high bulk modulus. As the system pressure reaches a critical value, the system bulk modulus is reduced considerably and a pressure plateau with a large volume change is formed. This dramatic volume change is due to the liquid infiltration into the nanopores. The initial pressure of the plateau, namely, the liquid infiltration pressure, is governed by the classic Laplace-Young equation as $P_{\rm in}$ = $2\Delta\gamma/r = 19$ MPa, where $\Delta\gamma$ is the excessive solid–liquid interfacial tension and r is the nanopore radius. With the increased system pressure, the gas molecules outside the nanopores are fully dissolved by the bulk liquid phase based on Henry's law, while the gas molecules inside the nanopores are fully dissolved by the confined liquid phase based on Henry's law and gas oversolubility. ^{25,28,29} When all the nanopores are filled with the liquid, the slope of the loading curve increases to a value slightly higher than its initial bulk modulus due to the reduced liquid amount outside of the nanopores. The accessible nanopore volume is determined by the width of the pressure plateau L_1 (Figure 2). The starting point of the infiltration plateau is defined as the point at which the slope of the loading curve is reduced by 50%, and the ending point is defined as the point at which the slope of the unloading curve is reduced by 50%.³⁰ The measured \hat{L}_1 (0.396 \pm 0.004 cm³/g) is almost the same as the nanopore volume measured by gas adsorption analysis, indicating that all the nanopores are invaded and fully filled by the liquid molecules during the pressure-induced liquid infiltration tests. The slight difference is due to the van der Waals distance between the liquid molecules and the hydrophobic surface of nanopores.³¹

Upon unloading, the pressure drops quickly with a slope similar to the initial elastic loading one. As the system pressure decreases to 10 MPa, the slope reduces and forms another pressure plateau, suggesting that the confined liquid as well as the dissolved gas molecules flows out from the hydrophobic nanopores. Simultaneously, with the reduced system pressure and the amount of liquid molecules confined in the nanopores, the gas molecules preserved in the nanopores precipitate out from the nanoconfined liquid and occupy the nanopore volume. The precipitated gas molecules are fully dissolved again when the liquid molecules infiltrate into the nanopores in the next loading process.

In the second cycle, the accessible nanopore volume L_2 is much reduced (Figure 2), indicating that only a part of the intruded liquid flows out of the nanopores during the unloading process in the first cycle. The variation in $P_{\rm in}$ is due to the partial liquid outflow and the pore size distribution of the silica gel. The degree of liquid outflow in the Nth cycle is determined as L_{N+1}/L_N . As shown in Figure 2, the degree of liquid outflow in the first cycle is 62.5%. From the second cycle, a 100% liquid outflow suggests that the LN system works as a stable energy absorber under consecutive loading—unloading conditions. The 100% liquid outflow from the second cycle decouples the gas—liquid interaction from liquid—solid interfacial tension and provides a baseline to further study the gas diffusion process in the nanopores.

3.2. Peak-Pressure-Holding Tests ($t_h > 0$). To study the unique gas diffusion behavior in the confined nanoenvironment, LN samples are held at the peak pressure at the end of the second loading process. Figure 3a shows the loading—

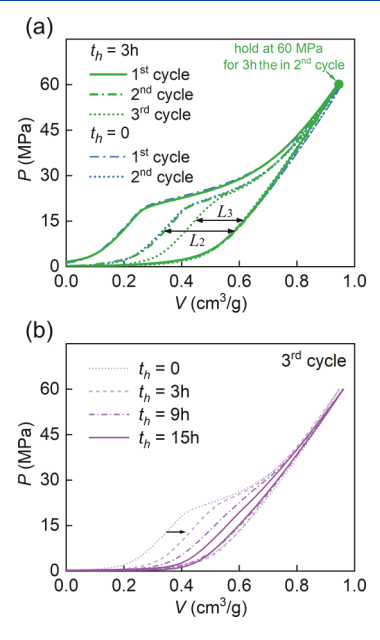


Figure 3. Typical loading—unloading curves of (a) LN sample with the 3 h peak-pressure-holding process and (b) third loading—unloading cycle of LN samples with various holding times.

unloading curves of an LN sample with a 3 h holding time. The first cycle and the loading curve of the second cycle are exactly the same as those in liquid infiltration tests without holding time. In the third cycle, the reduction in the plateau width indicates a much-reduced degree of liquid outflow during the unloading process of the second cycle.

As demonstrated in our previous studies, ^{21,25,26} the liquid outflow from hydrophobic nanopores is dominated by both the excessive solid–liquid interfacial tension and the gas–liquid

interaction in the nanopores during the unloading process. In all the liquid infiltration tests with or without the peak-pressure-holding process, the same liquid phase as well as the nanopore surface properties ensures a constant excessive solid—liquid interfacial tension. Thus, the much-reduced degree of liquid outflow is attributed to a time-dependent gas—liquid interaction during the peak-pressure-holding process, which promotes the gas to escape from the hydrophobic nanopores.

In the infiltration tests without the peak-pressure-holding process $(t_h = 0)$, the gas escape includes gas advection and gas diffusion from the nanopores to the bulk liquid during the unloading process. Given the unloading process completes in seconds, the amount of gas diffusion from the nanopores to the bulk liquid (a relatively slow process) can be ignored. The negligible gas diffusion is also validated by the same loadingunloading curves in the second and third cycles in Figure 2. Otherwise, a reduced L_3 should be observed. The gas advection describes the dissolved gas flowing out with the liquid and is proportional to the transfer velocity and total gas amount in the nanoconfined liquid. Since the system volume recovery speed (2 mm/min) and the unloading curves of the second and third cycles are the same, the initial transfer velocity of all LN samples is nearly the same. Therefore, the amount of gas molecules which escaped from the nanopores through advection is estimated as

$$n_{a} = \alpha \cdot n_{0} \tag{1}$$

where n_0 is the total amount of gas molecules dissolved in the nanoconfined liquid before the onset of the unloading process and α is ratio of the advected gas amount to the total gas amount. The amount of gas molecules preserved in the nanopores is

$$n_{p}^{t_{h}=0} = (1 - \alpha) \cdot n_{0} \tag{2}$$

While in the infiltration tests with the peak-pressure-holding process $(t_h = 3 \text{ h})$, the gas outflow includes the gas diffusion during the holding process and the gas advection during the unloading process. The amount of gas diffusion is denoted as n_d . The residual amount of gas molecules before the onset of the unloading process is $n_r = n_0 - n_d$. Consequently, the amount of gas molecules preserved in the nanopores is estimated as

$$n_{\rm p}^{t_{\rm h}>0} = (1-\alpha) \cdot n_{\rm r} \tag{3}$$

By comparing eqs 2 and 3, the amount of preserved gas molecules in the nanopores is reduced due to the gas diffusion during the peak-pressure-holding process. As the degree of liquid outflow is positively related to the amount of preserved gas molecules in the nanopores, ^{25,26}

$$\frac{n_{\rm r}}{n_0} = \frac{n_{\rm p}^{t_{\rm h}>0}}{n_{\rm p}^{t_{\rm h}>0}} \approx \frac{L_3^{t_{\rm h}>0}}{L_2} \tag{4}$$

Please note that n_0 is a constant as the nanopore volume, peak pressure, and initial gas content sealed in the testing cell are all constants for all the LN samples. As shown in Figure 3b, $L_{3\,\mathrm{h}}^{t\,>0}$ gradually decreases with increased holding time, which demonstrates the time-dependent gas diffusion process from the nanoconfined liquid phase to the bulk liquid one.

3.3. Pressure Effect on Gas Diffusion in Nanopores. To further study the effect of holding pressure on the behavior

of gas diffusion from the nanoconfined liquid phase to the bulk one, the peak pressure of the infiltration tests is increased from 60 to 150 MPa. Figure 4 shows typical loading—unloading

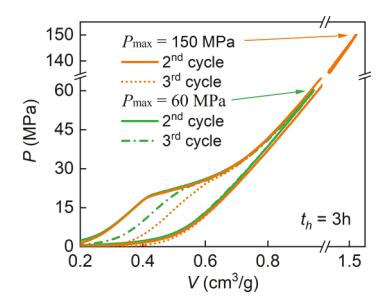


Figure 4. Typical loading—unloading curves of LN samples in 3 h peak-pressure-holding liquid infiltration tests with different peak pressures.

curves of 3 h peak-pressure-holding tests at different peak pressures. As L_2 is insensitive to the pressure increase, the excessive solid—liquid interfacial tension as well as the preserved gas molecules is identical for the LN system and independent of the peak pressure under continuous liquid infiltration testing cycles. After the peak-pressure-holding process in the second cycle, $L_3^{150\text{MPa}} < L_3^{60\text{MPa}}$ demonstrates the promoted gas diffusion rate at a higher holding pressure.

This pressure effect on gas diffusion in the nanoconfined liquid is not seen in the bulk liquid. In continuous theory, as described by Fick's second law, the diffusion rate is proportional to the diffusivity and the curvature of the concentration profile. According to the Wilke–Chang equation, 32 diffusivity is related to the density, molecular weight, and viscosity of the solvent, all of which are insensitive to pressure change. Therefore, the pressure effect on gas diffusion in the bulk liquid is negligible, which has also been demonstrated by both experimental and numerical studies. 14,33

Given that the diffusion path in the nanoporous particles and the initial gas concentration are the same for all LN samples before the onset of peak-pressure-holding, the pressure effect on gas diffusion is due to the enhanced diffusivity in the nanoenvironment. The enhanced diffusivity is attributed to the allocation of liquid and dissolved gas molecules in the hydrophobic nanopores. Under the hydrophobic nanoconfinement, gas molecules tend to be co-adsorbed with liquid molecules on the hydrophobic nanopore wall. As a result, the gas molecules are enriched in the adsorption layer, leading to the oversolubility of gas molecules, 18,35 which is much higher than the gas solubility around the center of the nanopores or in the bulk liquid phase (the green profile in Figure 5). This

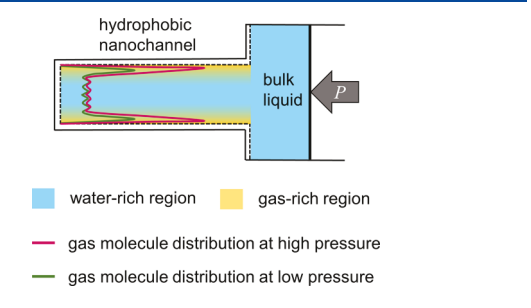


Figure 5. Schematic of the pressure effect on dissolved gas diffusion from the hydrophobic nanochannel to the bulk liquid.

oversolubility endows the adsorption layer to uptake more gas molecules than the nanopore center. In addition, as the system pressure increases, the spacing between the gas molecules is reduced and the system free energy is enhanced. The accumulation of gas molecules in the adsorption layer is energetically favorable and further promoted. Consequently, the gas concentration near the nanopore wall increases with the applied pressure, while the gas concentration at the nanopore center and in the bulk liquid phase is insensitive to the pressure increase (the red profile in Figure 5). This pressure-dependent gas concentration gradient between the adsorption layer in the hydrophobic nanopores and the bulk liquid phase leads to a higher gas diffusion rate.

3.4. Quantification of the Time- and Pressure-Dependent Gas Diffusion in the Nanoenvironment. Since n_0 is a constant, the gas diffusion during the peak-pressure-holding process can be simplified as the drive-in deposition. The concentration of gas molecules in this type of diffusion decays exponentially.³⁶ Therefore, to model the residual gas amount in the nanopores, exponential decay is applied as

$$\frac{n_{\rm r} - n_{\infty}}{n_0 - n_{\infty}} = \exp\left(-\frac{t}{\tau}\right) \tag{5}$$

where n_{∞} is the residual gas amount in the hydrophobic nanopores after the infinite holding process and τ is a constant.

As the experimental results cannot quantify the distribution of gas molecules along the nanopore depth, this simplified model is only capable of estimating the total amount of gas which retained in and flew out from the nanopores. Table 1 summarizes the experimental measurement of the degree of liquid outflow. Figure 6 shows the residual gas in the nanopores as a function of time under different peak pressures.

By fitting the experimental data, the parameters used in eq 5 are listed in Table 2. The residual gas amount shows a clear exponential decay trend. The time constant τ under 150 MPa is 3.3 h and much smaller than that under 60 MPa, indicating an enhanced gas diffusion rate under high pressure. The amount of residual gas in the nanopores after infinite diffusion time converges to a smaller value when the holding pressure is higher. This is attributed to the higher sensitivity of the gas oversolubility in the nanoconfined liquid phase to pressure increase, which facilitates the gas diffusion from the nanoconfined liquid phase to the bulk one. Both τ and n_{∞} reveal that the rate of dissolved gas diffusion out from hydrophobic nanopores is promoted by pressure. The convergence of the amount of residual gas in the nanopores also indicates that the gas molecules in the confined liquid and bulk liquid reach equilibrium and no further net gas diffusion occurs. A longer peak-pressure-holding process will lead to stabilized cyclic behavior.

4. CONCLUSIONS

In this work, we have investigated the dissolved gas diffusion from hydrophobic nanopores to the bulk liquid in an LN system by experimentally quantifying the change in the degree of liquid outflow. It has been found that as the holding time increases, the gas diffusion progresses exhibiting an exponentially decaying rate. In contrast to continuous theories, pressure has a prominent effect on the nanoscale gas diffusion. As pressure increases, the gas diffusion process from the nanoconfined liquid to the bulk liquid is significantly

Table 1. Measured Degree of Liquid Outflow in the Second Loading-Unloading Cycle $(L_1^{t_h>0}L_1)$

	holding time						
pressure (MPa)	0	1.5 h	3 h	6 h	9 h	12 h	15 h
60	100 ± 0	77.9 ± 2.4	73.0 ± 3.2	54.1 ± 5.7	36.1 ± 8.7	32.5 ± 5.1	22.9 ± 7.3
150	100 ± 0	65.1 ± 4.2	44.4 ± 2.5	32.9 ± 2.1	16.8 ± 2.2	15.1 ± 3.1	8.8 ± 7.6

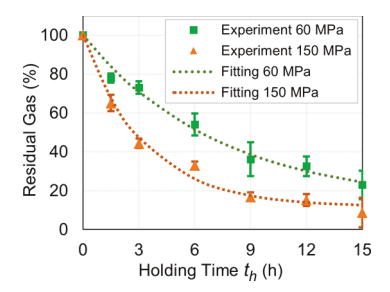


Figure 6. Preserved gas in the hydrophobic nanopores.

Table 2. Parameters in the Exponential Decay Model

pressure (Mpa)	n_{∞}/n_0 (%)	τ (h)	R^2 (%)
60	13.0	7.4	98.7
150	11.5	3.3	98.8

promoted. The pressure effect is related to the gas oversolubility and uneven distribution of gas and liquid molecules caused by the hydrophobic nanoconfinement. These findings extend the knowledge of the dissolved gas diffusion in a nanoenvironment and will guide the future design of CO2 sequestration and shale gas extraction systems.

ASSOCIATED CONTENT

Supporting Information

The Supporting Information is available free of charge at https://pubs.acs.org/doi/10.1021/acs.jpcc.0c11318.

> Loading-unloading cycle of an LN sample after the 3 h peak-pressure-holding test demonstrating the unchanged structural integrity and nanopore surface condition (PDF)

AUTHOR INFORMATION

Corresponding Author

Weiyi Lu - Department of Civil and Environmental Engineering, Michigan State University, East Lansing, Michigan 48824, United States; orcid.org/0000-0003-1069-3480; Phone: (517) 353-6448; Email: wylu@ egr.msu.edu

Authors

Lijiang Xu - Department of Civil and Environmental Engineering, Michigan State University, East Lansing, Michigan 48824, United States

Mingzhe Li - Department of Civil and Environmental Engineering, Michigan State University, East Lansing, Michigan 48824, United States

Complete contact information is available at: https://pubs.acs.org/10.1021/acs.jpcc.0c11318

Author Contributions

^TL.X. and M.L. contributed equally.

Notes

The authors declare no competing financial interest.

ACKNOWLEDGMENTS

The authors would like to thank Dr. Scott Calabrese Barton and Alex Mirabal for their help on the BET analysis. This work was financially supported by the National Science Foundation (CBET-1803695).

REFERENCES

- (1) Xu, H.; Yu, H.; Fan, J.; Zhu, Y.; Wang, F.; Wu, H. Two-Phase Transport Characteristic of Shale Gas and Water through Hydrophilic and Hydrophobic Nanopores. Energy Fuels 2020, 34, 4407-4420.
- (2) Sun, Z.; Shi, J.; Wu, K.; Li, X. Gas Flow Behavior through Inorganic Nanopores in Shale Considering Confinement Effect and Moisture Content. Ind. Eng. Chem. Res. 2018, 57, 3430-3440.
- (3) Phillips, R. K.; Friess, B. R.; Hicks, A. D.; Bellerive, J.; Hoorfar, M. Ex-Situ Measurement of Properties of Gas Diffusion Layers of PEM Fuel Cells. Energy Procedia 2012, 29, 486-495.
- (4) Nesbitt, N. T.; Burdyny, T.; Simonson, H.; Salvatore, D.; Bohra, D.; Kas, R.; Smith, W. A. Liquid-Solid Boundaries Dominate Activity of CO2 Reduction on Gas-Diffusion Electrodes. ACS Catal.. 2020, No. 10, 14093-14106, 10. DOI: 10.1021/acscatal.0c03319
- (5) Ho, T. A.; Wang, Y.; Xiong, Y.; Criscenti, L. J. Differential Retention and Release of CO2 and CH4 in Kerogen Nanopores: Implications for Gas Extraction and Carbon Sequestration. Fuel 2018,
- (6) Gadikota, G.; Dazas, B.; Rother, G.; Cheshire, M. C.; Bourg, I. C. Hydrophobic Solvation of Gases (CO2, CH4, H2, Noble Gases) in Clay Interlayer Nanopores. J. Phys. Chem. C 2017, 121, 26539-26550.
- (7) Bazhenov, S. D.; Lyubimova, E. S. Gas-liquid membrane contactors for carbon dioxide capture from gaseous streams. Petrol. Chem. 2016, 56, 889-914.
- (8) Ovcharova, A.; Vasilevsky, V.; Borisov, I.; Bazhenov, S.; Volkov, A.; Bildyukevich, A.; Volkov, V. Polysulfone Porous Hollow Fiber Membranes for Ethylene-Ethane Separation in Gas-Liquid Membrane Contactor. Sep. Purif. Technol. 2017, 183, 162-172.
- (9) Miachon, S.; Syakaev, V. V.; Rakhmatullin, A.; Pera-Titus, M.; Caldarelli, S.; Dalmon, J.-A. Higher Gas Solubility in Nanoliquids? ChemPhysChem 2008, 9, 78-82.
- (10) Soubeyrand-Lenoir, E.; Vagner, C.; Yoon, J. W.; Bazin, P.; Ragon, F.; Hwang, Y. K.; Serre, C.; Chang, J.-S.; Llewellyn, P. L. How Water Fosters a Remarkable 5-Fold Increase in Low-Pressure CO2 Uptake within Mesoporous MIL-100(Fe). J. Am. Chem. Soc. 2012, 134, 10174-10181.
- (11) Clauzier, S.; Ho, L. N.; Pera-Titus, M.; Coasne, B.; Farrusseng, D. Enhanced H2 Uptake in Solvents Confined in Mesoporous Metal-Organic Framework. J. Am. Chem. Soc. 2012, 134, 17369-17371.
- (12) Rakotovao, V.; Ammar, R.; Miachon, S.; Pera-Titus, M. Influence of the Mesoconfining Solid on Gas Oversolubility in Nanoliquids. Chem. Phys. Lett. 2010, 485, 299-303.
- (13) Moultos, O. A.; Tsimpanogiannis, I. N.; Panagiotopoulos, A. Z.; Economou, I. G. Atomistic Molecular Dynamics Simulations of CO2 Diffusivity in H2O for a Wide Range of Temperatures and Pressures. J. Phys. Chem. B 2014, 118, 5532-5541.
- (14) Cadogan, S. P.; Maitland, G. C.; Trusler, J. P. M. Diffusion Coefficients of CO2 and N2 in Water at Temperatures between 298.15 K and 423.15 K at Pressures up to 45 MPa. J. Chem. Eng. Data 2014, 59, 519-525.

- (15) Desbiens, N.; Demachy, I.; Fuchs, A. H.; Kirsch-Rodeschini, H.; Soulard, M.; Patarin, J. Water Condensation in Hydrophobic Nanopores. *Angew. Chem. Int. Ed.* **2005**, *44*, 5310–5313.
- (16) Giovambattista, N.; Rossky, P. J.; Debenedetti, P. G. Effect of Pressure on the Phase Behavior and Structure of Water Confined between Nanoscale Hydrophobic and Hydrophilic Plates. *Phys. Rev. E: Stat., Nonlinear, Soft Matter Phys.* **2006**, *73*, 041604.
- (17) Qiao, Y.; Cao, G.; Chen, X. Effects of Gas Molecules on Nanofluidic Behaviors. J. Am. Chem. Soc. 2007, 129, 2355-2359.
- (18) Li, W.; Nan, Y.; Zhang, Z.; You, Q.; Jin, Z. Hydrophilicity/ Hydrophobicity Driven CO2 Solubility in Kaolinite Nanopores in Relation to Carbon Sequestration. *Chem. Eng. J.* **2020**, 398, 125449.
- (19) Gao, Y.; Li, M.; Zhang, Y.; Lu, W.; Xu, B. Spontaneous Outflow Efficiency of Confined Liquid in Hydrophobic Nanopores. *Proc. Natl. Acad. Sci. U.S.A.* **2020**, *117*, 25246–25253.
- (20) Li, M.; Barbat, S.; Baccouche, R.; Belwafa, J.; Lu, W. Enhanced Energy Mitigation of Thin-Walled Tube Filled with Liquid Nanofoam under Dynamic Impact. *Compos. B Eng.* **2020**, *193*, 108047.
- (21) Li, M.; Xu, L.; Lu, W. Nanopore Size Effect on Critical Infiltration Depth of Liquid Nanofoam as a Reusable Energy Absorber. J. Appl. Phys. 2019, 125, 044303.
- (22) Zhang, Y.; Li, M.; Gao, Y.; Xu, B.; Lu, W. Compressing Liquid Nanofoam Systems: Liquid Infiltration or Nanopore Deformation? *Nanoscale* **2018**, *10*, 18444–18450.
- (23) Xu, B.; Qiao, Y.; Zhou, Q.; Chen, X. Effect of Electric Field on Liquid Infiltration into Hydrophobic Nanopores. *Langmuir* **2011**, 27, 6349–6357.
- (24) Sun, Y.; Li, P.; Qiao, Y.; Li, Y. Time-Dependent Gas-Liquid Interaction in Molecular-Sized Nanopores. Sci. Rep. 2014, 4, 6547.
- (25) Li, M.; Xu, L.; Lu, W. Effect of Extra Gas Amount on Liquid Outflow from Hydrophobic Nanochannels: Enhanced Liquid-Gas Interaction and Bubble Nucleation. *Langmuir* **2020**, *36*, 4682–4688.
- (26) Xu, L.; Li, M.; Lu, W. Effect of Electrolytes on Gas Oversolubility and Liquid Outflow from Hydrophobic Nanochannels. *Langmuir* **2019**, *35*, 14505–14510.
- (27) Li, M.; Lu, W. Liquid Marble: A Novel Liquid Nanofoam Structure for Energy Absorption. AIP Adv. 2017, 7, 055312.
- (28) Ho, L. N.; Schuurman, Y.; Farrusseng, D.; Coasne, B. Solubility of Gases in Water Confined in Nanoporous Materials: ZSM-5, MCM-41, and MIL-100. *J. Phys. Chem. C* **2015**, *119*, 21547–21554.
- (29) Battino, R.; Rettich, T. R.; Tominaga, T. The Solubility of Nitrogen and Air in Liquids. *J. Phys. Chem. Ref. Data* **1984**, *13*, 563–600
- (30) Zhan, C.; Li, M.; Lu, W. Functionalized Water Molecules Confined in Hydrogels for Energy Mitigation by Assembling Liquid Nanofoams in Micro Polymeric Pockets. *Compos. Commun.* **2020**, 20, 100357
- (31) Han, A.; Punyamurtula, V. K.; Qiao, Y. Effects of Cation Size on Infiltration and Defiltration Pressures of a MCM-41. *Appl. Phys. Lett.* **2008**, 92, 153117.
- (32) Wilke, C. R.; Chang, P. Correlation of Diffusion Coefficients in Dilute Solutions. *AIChE J.* **1955**, *1*, 264–270.
- (33) Michalis, V. K.; Moultos, O. A.; Tsimpanogiannis, I. N.; Economou, I. G. Molecular Dynamics Simulations of the Diffusion Coefficients of Light N-Alkanes in Water over a Wide Range of Temperature and Pressure. *Fluid Phase Equilib.* **2015**, 407, 236–242.
- (34) Ho, L. N.; Clauzier, S.; Schuurman, Y.; Farrusseng, D.; Coasne, B. Gas Uptake in Solvents Confined in Mesopores: Adsorption versus Enhanced Solubility. *J. Phys. Chem. Lett.* **2013**, *4*, 2274–2278.
- (35) Luzar, A.; Bratko, D. Gas Solubility in Hydrophobic Confinement. J. Phys. Chem. B 2005, 109, 22545–22552.
- (36) Abdel-Salam, A.; Chrysikopoulos, C. V. Analysis of a Model for Contaminant Transport in Fractured Media in the Presence of Colloids. *J. Hydrol.* **1995**, *165*, 261–281.